PLOS ONE

RESEARCH ARTICLE

Fabrication of 3-methoxyphenol sensor based on Fe_3O_4 decorated carbon nanotube nanocomposites for environmental safety: Real sample analyses

Mohammed M. Rahman[1,2]*, Mohammad Musarraf Hussain[1,2], Abdullah M. Asiri[1,2]

1 Chemistry Department, King Abdulaziz University, Jeddah, Saudi Arabia, **2** Center of Excellence for Advanced Material Research (CEAMR), King Abdulaziz University, Jeddah, Saudi Arabia

* mmrahman@kau.edu.sa

Citation: Rahman MM, Hussain MM, Asiri AM (2017) Fabrication of 3-methoxyphenol sensor based on Fe_3O_4 decorated carbon nanotube nanocomposites for environmental safety: Real sample analyses. PLoS ONE 12(9): e0177817. https://doi.org/10.1371/journal.pone.0177817

Editor: Yogendra Kumar Mishra, Institute of Materials Science, GERMANY

Received: November 27, 2016

Accepted: May 3, 2017

Published: September 22, 2017

Data Availability Statement: All relevant data are within the paper and its Supporting Information files.

Funding: The author(s) received no specific funding for this work.

Competing interests: The authors have declared that no competing interests exist.

Abstract

Iron oxide ornamented carbon nanotube nanocomposites (Fe_3O_4.CNT NCs) were prepared by a wet-chemical process in basic means. The optical, morphological, and structural characterizations of Fe_3O_4.CNT NCs were performed using FTIR, UV/Vis., FESEM, TEM; XEDS, XPS, and XRD respectively. Flat GCE had been fabricated with a thin-layer of NCs using a coating binding agent. It was performed for the chemical sensor development by a dependable I-V technique. Among all interfering analytes, 3-methoxyphenol (3-MP) was selective towards the fabricated sensor. Increased electrochemical performances for example elevated sensitivity, linear dynamic range (LDR) and continuing steadiness towards selective 3-MP had been observed with chemical sensor. The calibration graph found linear (R^2 = 0.9340) in a wide range of 3-MP concentration (90.0 pM ~ 90.0 mM). The limit of detection and sensitivity were considered as 1.0 pM and 9×10^{-4} $\mu A \mu M^{-1} cm^{-2}$ respectively. The prepared of Fe_3O_4.CNT NCs by a wet-chemical progression is an interesting route for the development of hazardous phenolic sensor based on nanocomposite materials. It is also recommended that 3-MP sensor is exhibited a promising performances based on Fe_3O_4.CNT NCs by a facile *I-V* method for the significant applications of toxic chemicals for the safety of environmental and health-care fields.

Introduction

The protection is a key apprehension in viewpoint of atmosphere and health that is a great issue to examine using sensors intended for the identification & recognition of toxic materials through an established practice. Semiconductor nanostructure material is very proficient and perceptive due to their high active surface area and different spherical morphologies to volume ratio in comparison with typical diameter from nano to micro ranges. In recent times, the nanostructure of metal oxide is an immense interest having their fascinating criteria such as fabrication of chemical sensor, dynamic surface area, elevated porosity, permeability, quantum confinement consequence, and stability [1–21]. Sensor based metal oxide conjugated carbon

composites are extensively used for the monitoring of air-water contamination, chemical process and poisonous constituents in the environment [22, 23]. Recognition and partition of contaminated resources from industrial waste water is one of the key issues in the biological and environmental field. Different methods reported for the isolation and removing of carcinogenic materials from the industrial waste water but a few issues are still remaining troubled that are removing of toxic agents in efficiently and re-usability of the NCs materials including their preparation at a facile and low cost. The mesoporous character of the NCs material allows a simplistic recycling devoid of foremost degradation of sensor effectiveness and potentiality. An excellent absorption and adsorption ability of the hybrid NCs, makes it's an appropriate sensor for the identification and removing of marked harmful agents from industrial and environmental wastes. Substituted and un-substituted phenols are common bi-products of industrial process having high toxicity properties. They are frequent contaminants in food, fresh and waste water [24]. 3-MP is an effective toxic element to environment and health. Hence it is very important to expand a suitable analytical process which is dependable, economical and efficient for the accurate quantification and sensitive finding of 3-MP. Various sensing techniques have been reported in the previous study to detect phenolic compounds such as electrochemical methods, HPLC and spectrometry. Among several detection methods, the electrochemical current—voltage (I-V*)* technique is a cheap, portable and easy to implement. Therefore, based on different nanostructure materials, semiconductor undoped or doped nanomaterials (NMs), transition metal oxides, electrocatalytic moieties, several chemically modified electrodes have been developed for the detection of 3-MP [25].

Diverse classes of nanoparticles (NPs), metallic or polymeric colloids used to improve the patient compliance and therapeutic efficiency of applicable medicines. Ferro-fluids are stable dispersions in water phase of magnetic iron-oxide NPs which have been studied in biomedical sciences as proficient device in *vitro* diagnosis, cell separation, immunoassays and nucleic acid concentration [26]. In chemically, iron oxide NPs have been used in NO reduction [27], adsorbents for heavy metals [28], pigments in cosmetic powders [29], anodes in lithium ion-batteries [30], detection of hydrogen peroxide [31], polymer coated of supra-magnetic NPs [32], application in magnetic resonance imaging [33], biomedical applications [34], imaging agents [35], photo-catalysis [36], removing of inorganic and organic pollutants [37], glycerol hydrogenolysis [38], hydrogenation of nitrobenzene [39], application in high-performance supercapasitor [40], catalytic oxidation [41], water treatment [42], separation of acid dye [43], antibody functionalization [44], biosensor applications [45], hybridization of nanotube [46], oil spill removing [47] and bio-distribution studies [48]. In this approach, Fe_3O_4.CNT NCs prepared by a simple wet-chemical process in alkaline phase, which revealed a steady growth development of NMs onto CNT surfaces and significantly executed for their potential applications. Fe_3O_4.CNT NCs have been used to fabricate a simple and efficient chemical sensor and assessed for the sensing performance selectively considering 3-MP in phosphate buffer (PB) at room temperature. To the best of our knowledge, this is the initial report for detection of 3-MP with prepared Fe_3O_4.CNT NCs onto GCE using an easy, suitable, and dependable I-V technique with short response time.

Experimental section

Materials and methods

The analytical grade chemicals such as acetone (Ac), 4-aminophenol (4-AP), ammonium hydroxide (NH_4OH), carbon nanotube (CNT), disodium phosphate (Na_2HPO_4), ethanol (EtOH), ferrous sulfate ($FeSO_4.7H_2O$), hydrazine (Hy), 3-methoxyphenol (3-MP), 4-methoxyphenol (4-MP), monosodium phosphate (NaH_2PO_4), nafion (5% ethanolic solution), *n*-hexane

(Hx), 2-nitrophenol (2-NP), sodium hydroxide (NaOH), tetrahydrofuran (THF), tolune-4-sulfonic acid hydrazide and xanthine (Xn), purchased from Sigma-Aldrich Company and used as received. FT-IR and UV/V spectra of the dried brown Fe_3O_4 NPs, and Fe_3O_4.CNT NCs were performed using Thermo scientific NICOLET iS50 FTIR spectrometer (Madision, WI, USA) and 300 UV/Visible spectrophotometer (Thermo scientific) respectively. The XPS measurements were examined to calculate the binding energy (eV) of C, Fe and O on a K-α spectrometer (Thermo scientific, K-α 1066) with an excitation radiation source (A1 Kα, Beam spot size = 300.0 μm; pass energy = 200.0 eV; pressure ~ 10^{-8} torr). The morphology and particle size of CNT, Fe_3O_4 NPs, and Fe_3O_4.CNT NCs were analyzed by FESEM and TEM (JEOL, JSM-7600F, Japan). XRD experiment was also carried out under ambient conditions to detect the crystalline pattern of Fe_3O_4.CNT NCs. *I-V* was performed [49, 50] to select 3-MP at a specific point by fabricated Fe_3O_4.CNT NCs using Keithley electrometer (6517A, USA) under room conditions.

Growth mechanism of Fe_3O_4.CNT NCs

Preparation of the Fe_3O_4.CNT nanocomposites is explained in detail and presented in the supporting information section (S1 Fig). In Fe_3O_4.CNT NCs growth method, initially Fe_3O_4 nucleus growth takes place by itself & mutual-aggregation, then nano-crystal re-aggregated and formed aggregated Fe_3O_4 nanocrystal using Ostwald-ripening method. Nanocrystal crystallizes and re-aggregates with each counter part in presence of disperse CNT through Vander-Waals forces and reformed Fe_3O_4 decorated CNT onto porous carbon nanotubes morphology, which presented in **Fig 1.**

Fabrication of glassy carbon electrode with Fe_3O_4.CNT NCs

NaH_2PO_4 (0.2 M, 39.0 mL), Na_2HPO_4 (0.2 M, 61.0 mL), and distilled water (100.0 mL) had been used for the preparation of PB (200.0 mL, 100.0 mM, pH = 7). Ethanol and conducting binder, nafion were used to fabricate GCE (surface area = 0.0316 cm^2) with Fe_3O_4.CNT NCs. After that, the fabricated electrode was kept at R. T. (3 h) for uniform film formation with completed drying. The fabricated GCE and platinum (Pt) were used as a working and counter electrode respectively in order to find out the I-V signals.

Results and discussion

Evaluation of optical and structural properties

The optical property is one of the important characteristics for the assessment of photo-catalytic activity of the brown grown Fe_3O_4 NPs and Fe_3O_4.CNT NCs. Based on UV/Vis. theory, the outer electrons of the atom absorb radiant energy and then shifted to the higher-energy levels. The spectrum including band-gap energy of the metal oxide can be achieved due to the

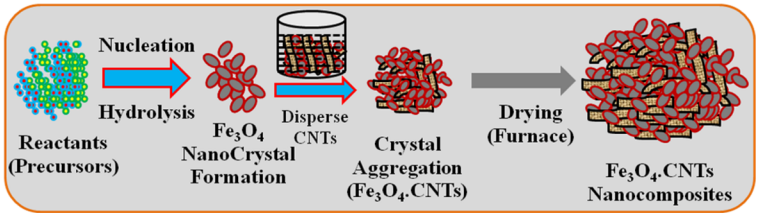

Fig 1. Schematic representation of growth mechanism of Fe_3O_4.CNTs NCs by a wet-chemical process.

https://doi.org/10.1371/journal.pone.0177817.g001

optical absorption. The UV/Vis. spectra of the Fe_3O_4 NPs and Fe_3O_4.CNT NCs were recorded in the visible range (200 ~ 800 nm). The absorption band at around 307.0 and 320.5 nm were found respectively (Fig 2A–2C). Based on the maximum level of band absorption, the band-gap energies of the Fe_3O_4 NPs and Fe_3O_4.CNT NCs were calculated using Tauc's equation (vi). Here, α = Absorption coefficient, A = Constant related to the effective mass of the electrons, r = 0.5 (Direct transition), E_g = Band-gap energy, h = Plank's constant, v = Frequency. Following the direct band-gap rule $(\alpha hv)^2 = A\,(hv\text{-}E_g)$, curve of $(\alpha hv)^2$ *vs* hv was plotted and then extrapolated to the axis. From the extrapolated curve, the band-gap energies for Fe_3O_4 NPs and Fe_3O_4.CNT NCs were found as 2.5 and 2.3 eV correspondingly (Fig 1B–1D) [51–53].

$$(\boldsymbol{\alpha hv})^{1/r} = \boldsymbol{A}(\boldsymbol{hv}-\boldsymbol{E_g}) \qquad \text{(vi)}$$

The CNT, Fe_3O_4 NPs and Fe_3O_4.CNTs NCs were also examined in perception of atomic and molecular vibrations to recognize the functional nature of the NCs using FTIR, and

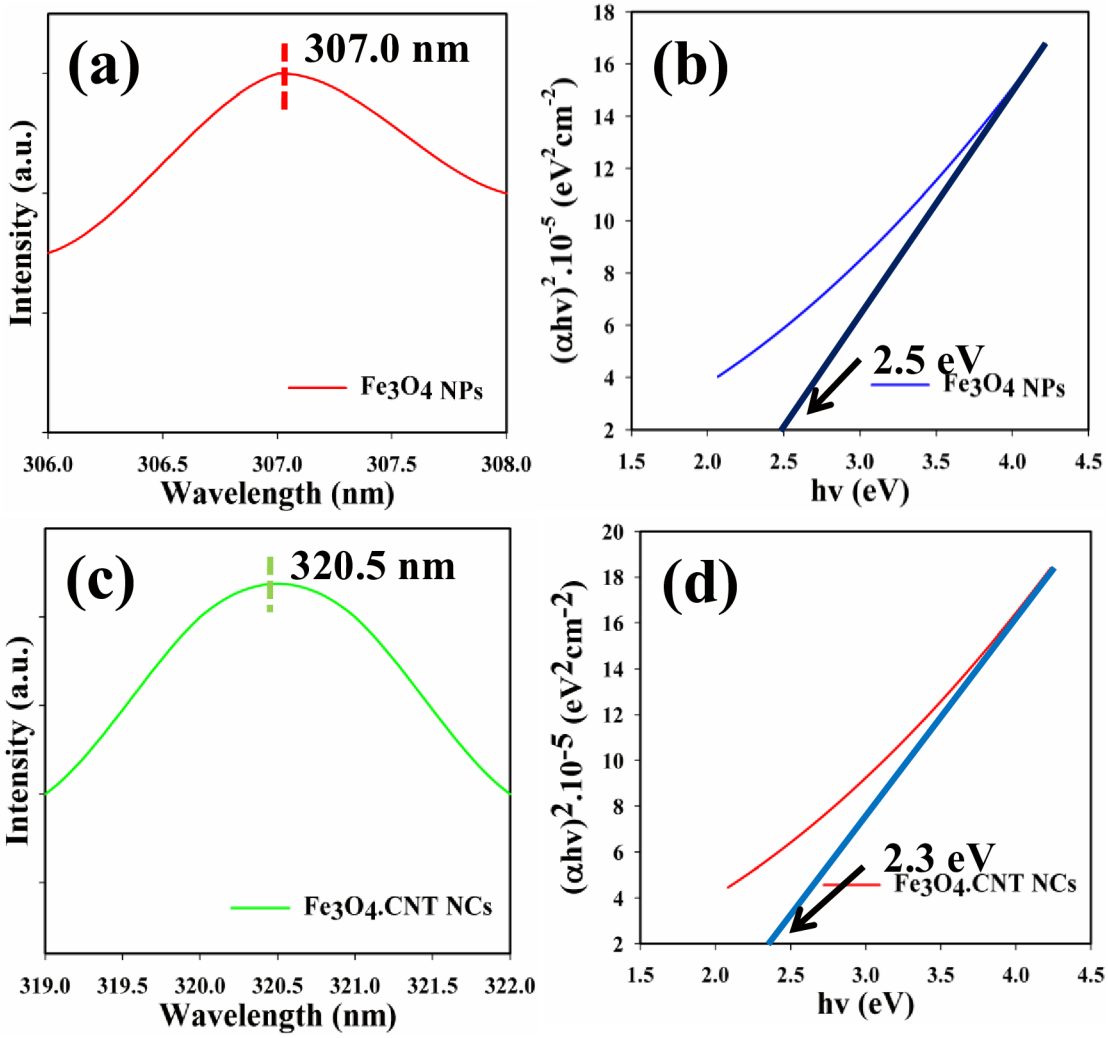

Fig 2. (a-c) UV/Vis spectra and (b-d) Band-gap energy plot of Fe_3O_4 NPs and Fe_3O_4.CNT NCs.

https://doi.org/10.1371/journal.pone.0177817.g002

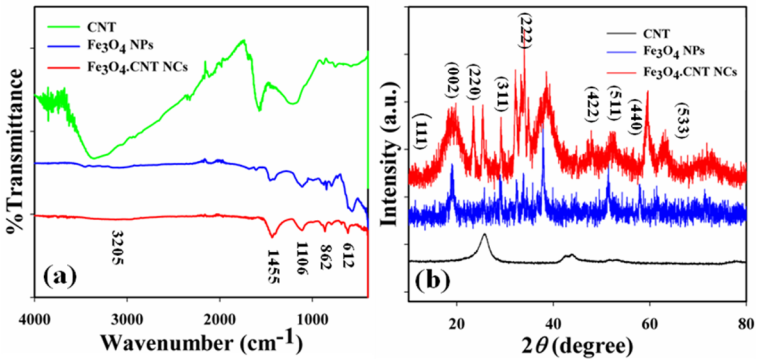

Fig 3. (a) FT-IR spectra, and (b) XRD patterns of CNT, Fe_3O_4 NPs and Fe_3O_4.CNT NCs.

https://doi.org/10.1371/journal.pone.0177817.g003

spectra were recorded in the region of 4000~400 cm^{-1} under room conditions. The FTIR spectra of the NCs shows peaks at 3205 (br), 1455 (s), 1106 (m), 862 (m) and 612 (m) cm^{-1} which recognized the presence of O-H (stretching), C–H (rocking), Fe–O–Fe (stretching), C–H and Fe = O (stretching) respectively (Fig 3A). The peak at 612 cm^{-1} indicates the formation of metal-oxide (Fe-O) bond which recognized the configuration of the Fe_3O_4 NPs and Fe_3O_4.CNT NCs [54].

Generally, the crystalline pattern indicates the metal-oxygen framework in nanostructure materials. XRD analysis was conducted to observe the crystalline nature of prepared Fe_3O_4. CNT NCs. The potential peaks with indication for 2θ values at 18.0 (111), 24.0, 25.5 (002), 29 (220), 32.0, 34.0 (311), 38.0 (222), 52.0 (422), 59.5 (511), 64.0 (440) and 73.0 (533) degrees (Fig 3B) were observed. All the pragmatic peaks in the spectra were assigned by using the JCPDS file (019–0629). The observed peak at 25.5 (002) was denoted for carbon of CNT and NCs. The strongest peak indicates the crystalline pattern and purity of the NCs. From the XRD analysis, it was suggested that a big amount of crystalline Fe_3O_4 was present in the synthesized iron oxide decorated CNT NCs [55].

Morphological and elemental characteristics

FESEM is one of the well-recognized processes to observe the morphology of the materials. The morphology and elemental analysis of the prepared brown Fe_3O_4.CNT NCs were measured using FESEM coupled-XEDS respectively. The typical shapes of CNT, Fe_3O_4 NPs, and brown Fe_3O_4.CNT NCs had been recorded from low to high magnified images (Fig 4A–4D). According to the magnified images, Fe_3O_4 was aggregated and decorated with a bright contrast along with well-dispersed onto the CNT surfaces. The conductance of CNT may be increased with the addition of Fe_3O_4 which correlated the calculation of band-gap energy (E_{bg}) of two different molecules.

Upon analysis of XEDS, oxygen (O) and iron (Fe) & carbon (C), oxygen (O) and iron (Fe) were found in the synthesized brown Fe_3O_4 NPs and Fe_3O_4.CNT NCs and contains O (6.93), Fe (93.07) & C (48.13), O (47.58) and Fe (4.30) wt% respectively. On the basis of FESEM equipped XEDS spectra, C are present in NCs but absent in NPs. There are no other peaks related with impurities were found in the spectra which indicated that the NCs are composed of C, O, and Fe only (Fig 5A–5D).

Determination of binding energy

XPS is a quantitative spectroscopic system which can be used to indicate the chemical nature of the elements present in the NCs. XPS spectra may be recorded by irradiating of an X-ray

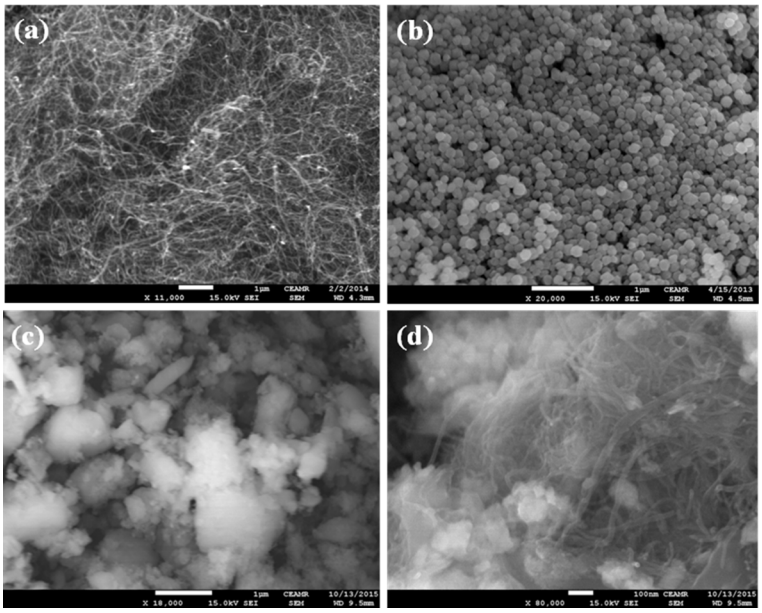

Fig 4. Magnified FESEM images (a) CNT, (b) Fe_3O_4 NPs, and (c-d) Fe_3O_4.CNT NCs.

https://doi.org/10.1371/journal.pone.0177817.g004

beam with a NCs material and kinetic energy including electrons number of the sample can be determined consecutively. According to the XPS spectra, carbon, oxygen and iron were found in the prepared Fe_3O_4.CNT NCs. A comparison between binding energies among CNT, Fe_3O_4 NPs and Fe_3O_4.CNT NCs are presented in **Table 1** and Fig 6A–6D [56].

TEM analysis

Additional morphological evaluation of Fe_3O_4.CNT nanocomposites was investigated by TEM analysis. It is revealed that the aggregated spherical-shaped Fe_3O_4 nanoparticle decorated onto CNT morphology, which is presented in Fig 7A and 7B. The TEM images (Fig 7A and 7B of

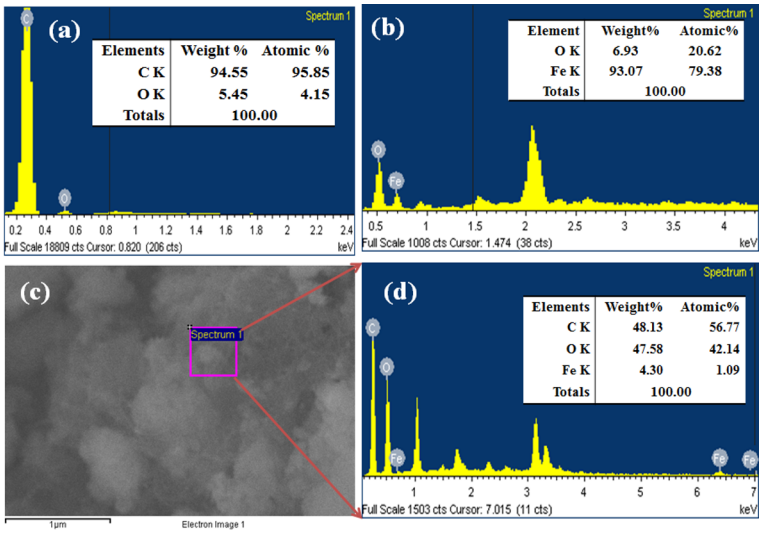

Fig 5. Elemental analysis (a) CNT, (b) Fe_3O_4 NPs, and (c-d) Fe_3O_4.CNT NCs.

https://doi.org/10.1371/journal.pone.0177817.g005

Table 1. Binding energies of NMs.

Elements	C1s	O1s	Fe^{2+} $2p_{3/2}$	Fe^{3+} $2p_{3/2}$	Fe^{2+} $2p_{1/2}$	Fe^{3+} $2p_{1/2}$
CNT	285.0	-	-	-	-	-
Fe_3O_4 NPs	-	553.0	712.0	717.0	728.0	734.0
Fe_3O_4.CNT NCs	289.7	535.4	710.3	716.4	721.2	725.1

https://doi.org/10.1371/journal.pone.0177817.t001

Fe_3O_4 NPs decorated nanocomposites of CNT were showed the existence of aggregated Fe_3O_4 nanoparticle adsorption onto the surface of CNTs nanocomposites. In the TEM images, it displays the actual morphology of the various nanocomposites assembled in spherical-shaped Fe_3O_4-particle-like morphology decorated CNT, which correspondence to the adsorption as well as aggregation of nanocomposite materials.

Application

Detection of 3-methoxyphenol by Fe_3O_4.CNT NCs

Enhancement of the fabricated electrode with NCs is the initial stage of using as a chemical sensor. The significant application of Fe_3O_4.CNT NCs is assembled onto GCE as a chemical sensor, which carried out for the detecting and measuring of target agent, 3-MP in PB. The Fe_3O_4.CNT NCs/GCE sensor have more advantages for example chemically inert, safe, electro-chemical activity, easy to fabricate, non-toxic, simple to assemble and stable in air. According to the I-V method, the current responses of Fe_3O_4.CNT NCs/GCE were considerably changed during 3-MP adsorption. A significant amplification in the current response with applied potential was noticeably confirmed having the holding time of electrometer was 1.0

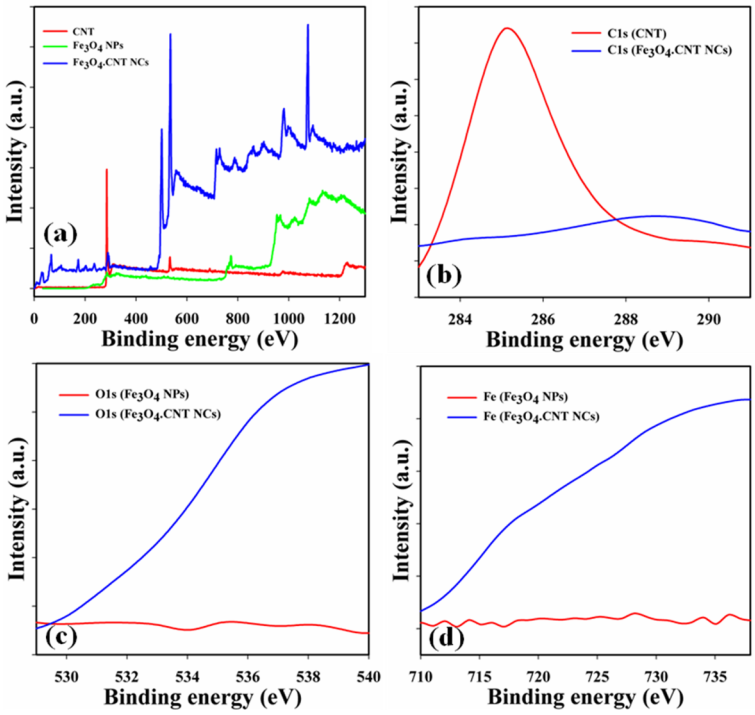

Fig 6. XPS study of CNT, Fe_3O_4 NPs, and Fe_3O_4.CNT NCs (a) Full spectrum, (b) C1s level, (c) O1s, and (d) Fe^{2+} $2p_{3/2}$ and Fe^{2+} $2p_{1/2}$ level.

https://doi.org/10.1371/journal.pone.0177817.g006

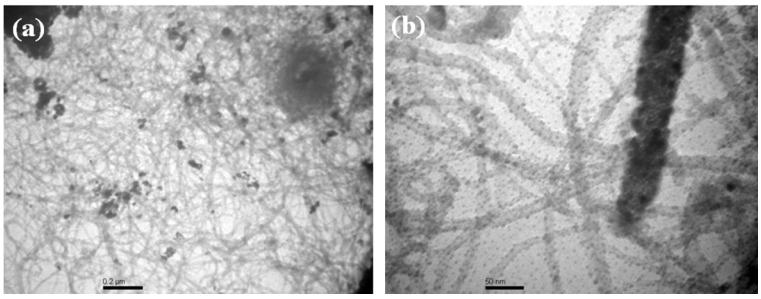

Fig 7. TEM analysis of Fe_3O_4.CNT nanocomposites (a-b) Low-to-high magnified images.

https://doi.org/10.1371/journal.pone.0177817.g007

sec. The overall possible mechanism of 3-MP detection by Fe_3O_4.CNT NCs using I-V technique is presented in Fig 8.

The potential application of Fe_3O_4.CNT NCs assembled onto an electrode as a chemical sensor has been engaged for the identification of compounds that are biological and environmentally hazardous. The current responses (potential range: 0 ~ +1.5 V) for the bare, GCE with nafion, and coated with Fe_3O_4.CNT NCs on the working electrode surface were presented in Fig 9A**.** The differences of the current responses between bare and coated GCE occurred due to the current signals were enhanced by coated electrode in compared with bare GCE. The current signal without (red-dotted) and with (black dotted) analyte were recorded (Fig 9B). A significant improvement of current responses occurred in case of the modified Fe_3O_4.CNT electrode with 3-MP which gives a higher surface area with better coverage in absorption and adsorption potentiality onto the porous NCs surfaces of the target compound (3-MP). The I-V responses of the 3-MP with different concentration (90 pM ~ 90 mM) towards Fe_3O_4.CNT NCs modified electrode were recorded which signified that the changes of current of the fabricated electrode was a function of 3-MP concentration under normal condition and it was also revealed that the current responses increased regularly from lower to higher concentration of the target molecule (Fig 9C). A broad range of the analyte concentrations were measured from the lower to higher potential (0.0 ~ 1.5 V) to examination of the possible analytical limit. The linear calibration curve at 0.8 V were plotted from the various concentrations of 3-MP (90 pM ~ 90 mM). The LDR (90 pM ~ 90 nM), regression co-efficient (R^2 = 0.9340), sensitivity

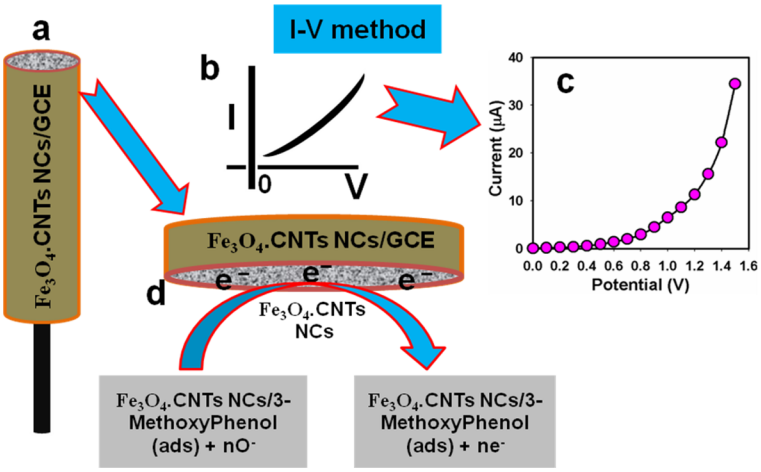

Fig 8. Schematic view (a) Coated rod-shape round disc-GCE, (b) Expected *I-V* curve, (c) Observed *I-V* response, (d) Proposed detection mechanism of 3-MP by Fe_3O_4.CNT NCs/GCE.

https://doi.org/10.1371/journal.pone.0177817.g008

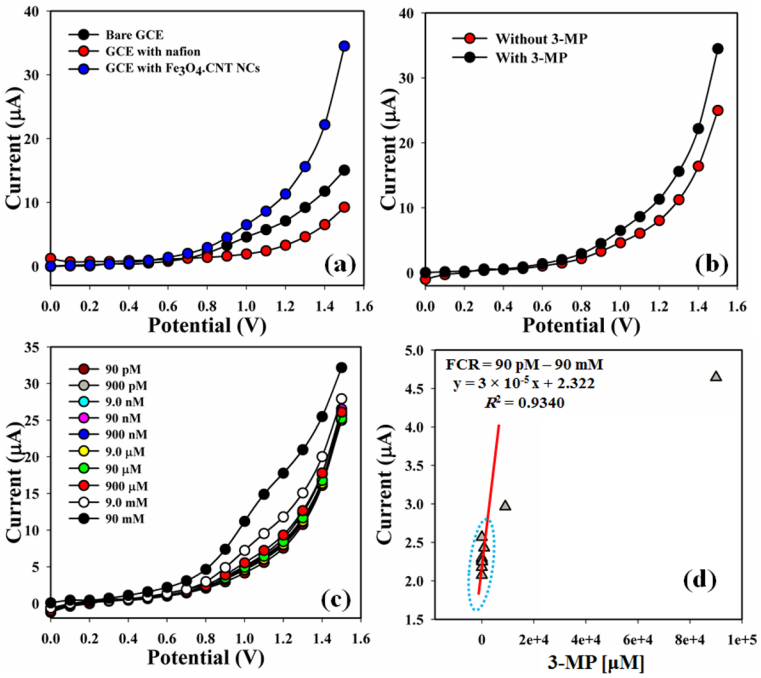

Fig 9. Current-voltage responses of Fe_3O_4.CNT NCs (a) Bare and coated electrode, (b) Absence and presence of 3-MP, (c) Concentration variation of the 3-MP and (d) Calibration curve.

https://doi.org/10.1371/journal.pone.0177817.g009

(9×10^{-4} μAμM^{-1}cm^{-2}), and LOD (1.0 pM) at signal to noise ratio ~ 3 were calculated from the calibration curve (Fig 9D). Response time (r. t. = 11 s) of the electrode was calculated from the practical concentration variation graph (Fig 10A).

The resistance value of the Fe_3O_4.CNT NCs modified GCE chemical sensor can be decreased with increasing active surface area which is an important property of the growth NCs particles [57]. These reactions could be occurred in bulk-system/air-liquid interface/ neighboring atmosphere owing to the small carrier concentration, which increased the resistance during increasing the electrical properties. For enhancement of the oxygen adsorption, the sensitivity/conductivity of 3-MP towards Fe_3O_4.CNT NCs could be ascribed having higher-oxygen lacking conducts. Larger amount of oxygen adsorbed on the Fe_3O_4-doped NCs sensor surface, higher would be the oxidizing potentiality and faster would be the oxidation of 3-MP and higher would be the resultant current. The activity of 3-MP would have been extremely big as contrast to other toxic chemical with the surface under indistinguishable conditions [58, 59]. In two-electrode system, I-V characteristic of the Fe_3O_4.CNT NCs coated GCE is activated as a function of 3-MP concentration at room conditions, where improved current response was observed. As obtained, the current response of the Fe_3O_4.CNT NCs/ GCE film was increased with the increasing concentration of 3-MP; however similar phenomena for toxic chemical detection have also been reported earlier [60–62]. At a low concentration of 3-MP in liquid medium, there is a smaller surface coverage of 3-MP molecules on Fe_3O_4.CNT NCs/GCE film and hence the surface reaction proceeds steadily. By increasing the 3-MP concentration, the surface reaction is increased significantly (gradually increased the response as well) owing to large surface area contacted with 3-MP molecules. Further increasing of 3-MP concentration on Fe_3O_4.CNT NCs/GCE surface, it was exhibited a more rapid increased of current responses, due to larger surface covered by 3-MP. The 3-MP sensing mechanism of the Fe_3O_4.CNT NCs/GCE fabricated film is explained and presented in

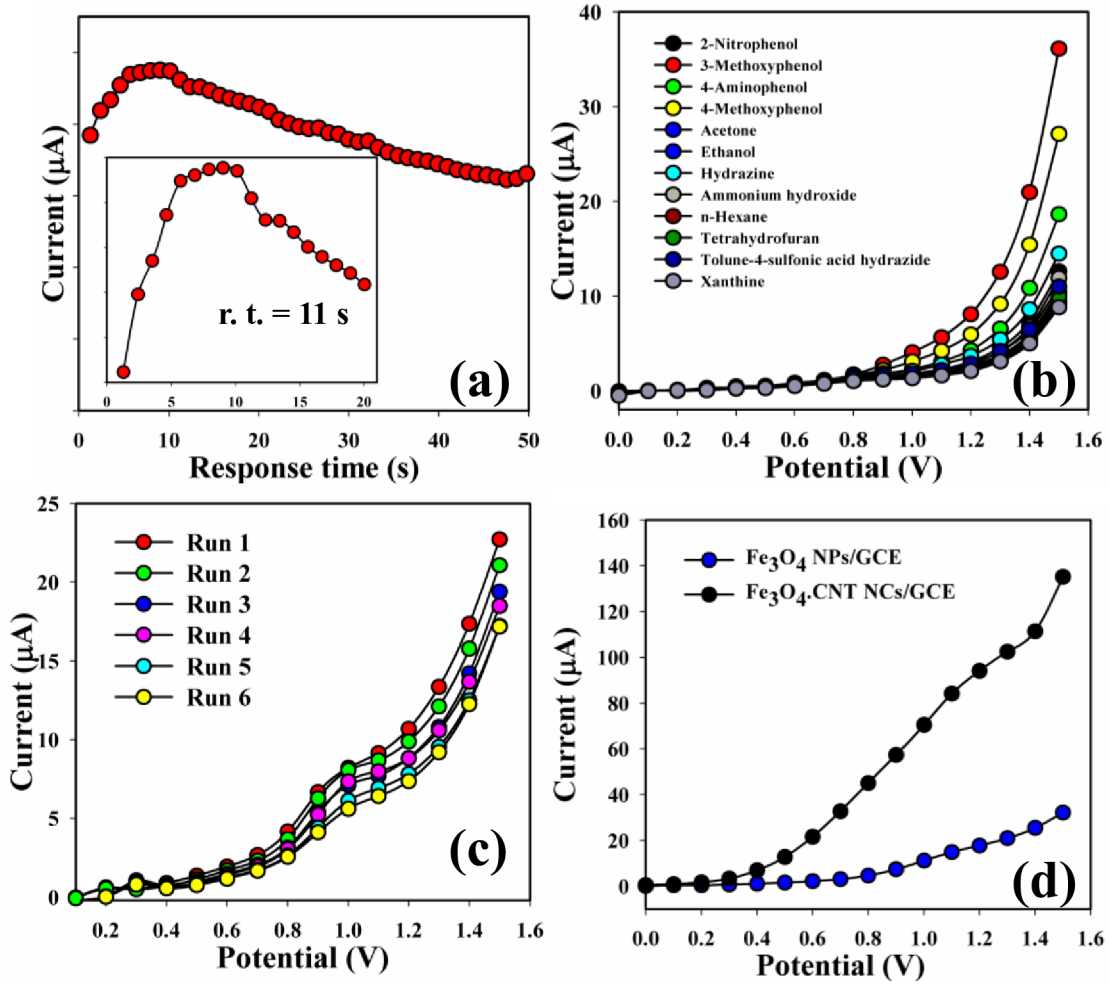

Fig 10. (a) Response time, (b) Selectivity, (c) Reproducibility study, and (d) Control experiment.

https://doi.org/10.1371/journal.pone.0177817.g010

reactions [vii—ix]. Where, oxygen (dissolved) is chemisorbed on the Fe_3O_4.CNT NCs/GCE surfaces, when the porous-fabricated-film is immersed in PB. During the chemical adsorption, the dissolved oxygen is transferred into ionic species such as O_2^- and O^- which gained electrons from the conduction band.

$$\mathbf{O_{2(diss)} \rightarrow O_{2(ads)}} \quad \text{(vii)}$$

$$\mathbf{O_{2(ads)} + e^- \rightarrow {O_2}^-_{(ads)}} \quad \text{(viii)}$$

$$\mathbf{{O_2}^-_{(ads)} + e^- \rightarrow 2{O}^-_{(ads)}} \quad \text{(ix)}$$

The reaction between 3-MP and ionic oxygen species can take place in (x), and the reaction is depended on the concentration of 3-MP in the medium. On Fe_3O_4.CNT NCs/GCE surfaces, 3-MP oxidized and then electrons were released into the conduction band, therefore decreased the resistance and consequently increased the transmission current.

$$\mathbf{3-MP\ (ad-ox/Fe_3O_4.CNT) + n{O}^-_{(ads)} \rightarrow 3-MP\ (de-red/Fe_3O_4.CNT) + ne^-} \quad \text{(x)}$$

Table 2. Detection of phenols using different electrochemical approach.

Electrode	Methods	Phenols	Sensitivity ($\mu A \mu M^{-1} cm^{-2}$)	LOD (pM)	LDR (mM)	Ref.
POAS-Ag/MWCNT/GCE	I-V	3-MP	3.829 $\mu AmM^{-1}cm^{-2}$	360	0.4–40.0	[24]
NiO.CNT/GCE	I-V	4-AP	6.33×10^{-4}	15	-	[49]
Graphene-polyaniline/GCE	DPV	4-AP	1.776042	0.065 mM	0.2–20, 20–100	[63]
RGO/P-$_L$-GSH/GCE	AM	4-AP	27.2	0.03 mM	0.4–200	[64]
Ce_2O_3.CNT/GCE	I-V	2-NP	1.6×10^{-3}	60	100.0 pM -100.0 μM	[65]
Fe_3O_4.CNT NCs/GCE	**I-V**	**3-MP**	**9.49×10^{-4}**	**1.0**	**90 pM– 90 nM**	**This work**

4-AP = 4-Aminophenol, AM = Amperometry, 3-MP = 3-Methoxyphenol, 2-NP = 2-Nitrophenol.

https://doi.org/10.1371/journal.pone.0177817.t002

Response time was measured by Fe_3O_4.CNT NCs/GCE in presence target 3-MP analyte and presented in Fig 10A. The selectivity was performed with different chemicals such as 2-NP, 3-MP, 4-AP, 4-MP, Ac, EtOH, Hy, NH_4OH, Hx, THF, tolune-4-sulfonic acid, hydrazide, and Xn. 3-MP showed maximum current responses towards Fe_3O_4.CNT NCs fabricated electrode and therefore it was clearly reported that the sensor was most selective to 3-MP compared with other chemicals (Fig 10B). The sensitivity of the Fe_3O_4.CNT NCs coated electrode sensor was performed up to two weeks for the examination of the reproducible and storage capabilities. It was recognized that the I-V responses were not significantly changes after washing of each experiment of the fabricated Fe_3O_4.CNT NCs electrode (Fig 10C).

The sensitivity remained almost equal as the initial response up to two weeks and after that the responses of the fabricated electrode become decreased gradually. A series of six successive measurements of 3-MP solution (900 nM) yielded good reproducible responses with the Fe_3O_4.CNT NCs electrode at different conditions. A control experiment was also performed at 3-MP concentration (900 mM) with different fabricated electrodes and a remarkable increased of current response was found for the Fe_3O_4.CNT NCs compared with Fe_3O_4 NPs (Fig 10D). The responses of NCs sensor were determined with respect to storage time for measurement of long term storage capacity. The storage stability measurement of the Fe_3O_4.CNT NCs electrode sensor was conducted under normal conditions and the sensitivity remained almost 90% as the initial responses for several days. It was clearly denoted that the fabricated sensor may be used without any significant degradation of sensitivity up to several weeks. The sensor performances using different electrochemical approach toward phenolic derivatives have been concluded [24, 49, 63–65] in Table 2.

Table 3. Measurement of 3-MP using modified Fe_3O_4.CNT NCs/GCE.

Real samples	Observed current (μA)				Conc. (μM)	SD
	R1	R2	R2	Average		(n = 3)
Industrial effluent	7.09	5.27	4.91	5.75	23.76	1.17
PC baby bottle	7.73	5.25	4.42	5.80	23.96	1.72
PC bottle safa	1.66	4.14	3.85	3.22	13.30	1.36
PVC food packaging bag	4.18	3.08	2.77	3.34	13.80	0.74
Red sea water	4.33	3.31	2.58	3.41	14.09	0.88
Tape water	3.54	2.66	2.31	2.83	11.71	0.63

R = Reading, SD = Standard deviation

https://doi.org/10.1371/journal.pone.0177817.t003

Real sample analysis

On the subject of authentication of the legitimacy of I-V system, the Fe_3O_4.CNT NCs/GCE used to detect the 3-MP in different original samples. A standard addition method used to approximate the concentration of 3-MP in real samples that were collected from diverse sources. A set amount (~25.0 μL) of every original analyte mixed and examined in PB (10.0 mL) using fabricated Fe_3O_4.CNT NCs/GCE. The obtained results concerning 3-MP finding are presented in Table 3, and actually established that the anticipated Fe_3O_4.CNT NCs/GCE advancement is acceptable, dependable, and proper for analyzing real samples using I-V design.

Conclusion

Fe_3O_4.CNT NCs were prepared using an easy, efficient and simple wet-chemical method in basic medium. The electrochemical characteristic of NCs was performed by UV/Vis, FT-IR, FESEM, XEDS, XPS and XRD techniques. A simple fabrication method used to fabricate Fe_3O_4.CNT NCs thin-film onto flat GCE electrode. The sensitive and selective of 3-MP sensor was prepared successfully based on GCE embedded with Fe_3O_4.CNT NCs by conducting coating binder. The electrochemical investigation of the fabricated 3-MP sensor was excellent in point of detection limit including linear-dynamic range, sensitivity and response time. The Fe_3O_4.CNT NCs/GCE exhibited higher sensitivity (9×10^{-4} $\mu AmM^{-1}cm^{-2}$) and lower detection limit (1.0 pM) by considering the signal-to-noise ratio of 3. A well-established route can be introduced from this novel approach for the development of efficient chemical sensor for biological and environmental toxin in a broad scale.

Supporting information

S1 Fig. Preparation of nanocomposites from Fe_3O_4 NPs and CNT.
(DOCX)

Acknowledgments

Center of Excellence for Advanced Materials Research (CEAMR), King Abdulaziz University, Jeddah is acknowledged for instrumental support.

Author Contributions

Conceptualization: MMR.

Data curation: MMR.

Formal analysis: MMH MMR.

Funding acquisition: AMA.

Investigation: MMH MMR.

Methodology: MMH MMR.

Project administration: MMR AMA.

Resources: MMR AMA.

Software: MMH MMR.

Supervision: MMR AMA.

Validation: MMH MMR.

Visualization: MMH MMR.

Writing – original draft: MMH MMR.

Writing – review & editing: MMR AMA.

References

1. Rahman MM, Asiri AM, Fabrication of highly sensitive ethanol sensor based on doped nanostructure materials using tiny chips. RSC Adv. 2015; 5:63252.
2. Snure MA, Tiwari, Band-gap engineering of Zn1-x Gax O nanopowders: Synthesis, structural and optical characterizations. J. Appl. Phys. 2008; 104:073707.
3. Snure MA, Tiwari, Synthesis, Characterization, and Green Luminescence in ZnOnanocages. J. Nanosci. Nanotech. 2007; 7:481.
4. Rahman MM, Asiri AM, Electrochemical Sensors Technology. InTech Open Access publisher 2017.
5. Tian K, Alex S, Siegel G, Tiwari A, Enzymatic glucose sensor based on Au nanoparticle and plant-like ZnO film modified electrode. Mater. Sci. Engr. C 2015; 46:548.
6. Schuchardt A, Braniste T, Mishra YK, Deng M, Mecklenburg M, Stevens-Kalceff MA, Three-dimensional Aerographite-GaN hybrid networks: Single step fabrication of porous and mechanically flexible materials for multifunctional applications. Sci. Rep. 2015; 5:8839. https://doi.org/10.1038/srep08839 PMID: 25744694
7. Garlof S, Fukuda T, Mecklenburg M, Smazna D, Mishra YK, Adelung R, Electro-mechanical piezoresistive properties of three dimensionally interconnected carbon aerogel (Aerographite)-epoxy composites. Composites Sci. Technol. 2016; 134:226.
8. Balkhoyor HB, Rahman MM, Asiri AM, Chemical sensors based on nanostructure materials. LAMBERT Academic Publishing 2017; 1–232.
9. Garlof S, Mecklenburg M, Smazna D, Mishra YK, Adelung R, Schulte K, 3D carbon networks and their polymer composites: Fabrication and electromechanical investigations of neat Aerographite and Aerographite-based PNCs under compressive load. Carbon 2017; 111:103.
10. Rahman MM, Alam MM, Asiri AM, Islam M.A., Fabrication of selective chemical sensor with ternary $ZnO/SnO_2/Yb_2O_3$nanoparticles. Talanta 2017; 170:215. https://doi.org/10.1016/j.talanta.2017.04.017 PMID: 28501161
11. Rahman MM, Ahmed J, Asiri AM, Development of creatine sensor based on antimony-doped tin oxide (ATO) nanoparticles. Sens. Actuators B 2017; 242:167.
12. Balkhoyor HB, Rahman MM, Asiri AM, Effect of Ce-doping into ZnO nanostructures to enhance the phenolic sensor performances. RSC Adv. 2016; 6: 58236.
13. Khan SB, Rahman MM, Akhtar K, Asiri AM, Rub AM, Nitrophenol cemi-sensor and active solar photocatalyst based on spinel hetaerolite nanoparticles. PLoS ONE 2014; 9:e85290. https://doi.org/10.1371/journal.pone.0085290 PMID: 24465525
14. Rahman MM, Ahmed J, Asiri AM, Hasnat M.A., Siddiquey I.A., Development of 4-methoxyphenol chemical sensor based on NiS_2-CNT nanocomposites. J. Taiwan Institute of Chem. Engr. 2016; 64:157.
15. Rahman MM, Abu-Zied BM, Hasan MM, Asiri AM, Hasnat MA, Fabrication of selective 4-aminophenol sensor based on H-ZSM-5 zeolites deposited silver electrodes. RSC Adv. 2016; 6:48435.
16. Alam MK, Rahman MM, Abbas M, Torati SR, Asiri AM, Kim D, Ultra-sensitive 2-nitrophenol detection based on reduced graphene oxide/ZnO nanocomposites. J. Electroanal. Chem. 2017; 788:66.
17. Rahman MM, Balkhoyor HB, Asiri AM, Phenolic sensor development based on chromium oxide-decorated carbon nanotubes for environmental safety. J. Environ. Management 2017; 188:228.
18. Lupan O, Postica V, Wolff N, Polonskyi O, Duppel V, Kaidas V, et al, Localized Synthesis of Iron Oxide Nanowires and Fabrication of High Performance Nanosensors Based on a Single Fe_2O_3 Nanowire. Small 2017; 13:1602868.
19. Qu J, Dong Y, Wang Y, Xing H, A novel sensor based on Fe_3O_4 nanoparticles–multiwalled carbon nanotubes composite film for determination of nitrite. Sens. Bio-Sens. Res. 2015; 3:74.
20. Rahman MM, Nanomaterials. Intech open access publisher 2011; 1–356.
21. Tiginyanu I, Ghimpu L, Grottrup J, Postolache V, Mecklenburg M, Stevens-Kalceff MA et al, Strong light scattering and broadband (UV to IR) photoabsorption in stretchable 3D hybrid architectures based on

Aerographite decorated by ZnO nanocrystallites. Sci. Rep. 2016; 6:32913. https://doi.org/10.1038/srep32913 PMID: 27616632

22. Xu JQ, Han JJ, Zhang Y, Sun YA, Xie B, Studies on alcohol sensing mechanism of ZnO based gas sensors. Sens. Actuators B 2008; 132:334.
23. Nissim R, Compton RG, Introducing absorptive stripping voltammetry: wide concentration range voltammetirc phenol detection. Analyst 2014; 139:5911. https://doi.org/10.1039/c4an01417k PMID: 25244304
24. Rahman MM, Khan A, Asiri AM, Chemical sensor development based on poly (*O*-anisidine)silverized-MWCNT nanocomposites deposited on glassy carbon electrodes for environmental remediation. RSC Adv. 2015; 5:71370.
25. Rahman MM, Jamal A, Khan SB, Faisal M, Fabrication of Highly Sensitive Ethanol Chemical Sensor Based on Sm-Doped Co_3O_4 Nanokernels by a Hydrothermal Method. J. Phys. Chem. C 2011; 115:9503.
26. Su Y, Zhao B, Deng W, NO reduction by methane over iron oxides: Characteristics and mechanisms. Fuel 2015; 160:80.
27. Zhang C, Yu Z, Zeng G, Huang B, Dong H, Huang J, et al, Phase transformation of crystalline iron oxides and their adsorption abilities for Pb and Cd. Chem. Engr. J. 2016; 284:247.
28. Wawrzynczak A, F-Guzik A, Nowak I, Mesoporous silica films with accessible pore structures on iron oxide. Dyes Pigments 2016; 124:27.
29. Jang B, Chae OB, Park S-K, Ha J, Oh SM, Na H, et al, Solvent less synthesis of an iron-oxide/grapheme nanocomposite and its application as an anode in high rate Li-ion batteries. J. Mater. Chem. A 2013; 1:15442.
30. Lin C-Y, Chang C-T, Iron oxide nanorods array in electrochemical detection of H_2O_2. Sens. Actuators B 2015; 220:695.
31. Chen S, Raynolds F, Yu L, Weissleder R, Josephson L, A screening paradigm for the design of improved polymer-coated supramagnetic iron oxide nanoparticles. J. Mater. Chem. 2009; 19:6387.
32. Qiao R, Yang C, Gao M, Supramagnetic iron oxide nanoparticles: from preparations to in *vivo* MRI applications. J. Mater. Chem. 2009; 19:6274.
33. Amstad E, Textor M, Reimhult E, Stabilization and functionalization of iron oxide nanoparticles for biomedical applications. Nanoscale 2011; 3:2819. https://doi.org/10.1039/c1nr10173k PMID: 21629911
34. Herman DAJ, Ferguson P, Cheong S, Hermans IF, Ruck BJ, Allan KM, et al, Hot-injection synthesis of iron/iron oxide core/shell nanoparticles for T_2 contrast enhancement in magnetic resonance imaging. Chem. Commun. 2011; 47:9221.
35. Nolan M, Electronic coupling in iron-oxide-modified TiO_2 leads to a reduced band gap and charge separation for visible light active photo-catalysis. Phys. Chem. Phys. Chem. 2011; 13:18194.
36. Yang X, Chen C, Li J, Zhao G, Ren X, Wang X, Grapheme oxide-iron oxide and reduced graphene oxide-iron oxide hybrid materials for the removal of organic and inorganic pollutants. RSC Adv. 2012; 2:8821.
37. Ge J, Zheng Z, Liao F, Zheng W, Hong X, Tsang SCE, Palladium on iron oxide nanoparticles: the morphological effect of the support in glycerol hydrogenolysis, Green Chem. 2013; 15:2064.
38. Easterday R, S-Felix O, Losovyj Y, Pink M, Stein BD, Morgan DG, et al, Design of ruthenium/iron oxide nanoparticle mixtures for hydrogenation of nitrobenzene, Catal. Sci. Technol. 2015; 5:1902.
39. Mitchell E, Gupta RK, M-Darkwa K, Kumar D, Ramasamy K, Gupta BK, et al, Facile synthesis and morphogenesis of superparamagnetic iron oxide nanoparticles for high-performance supercapacitor applications. New J. Chem. 2014; 38:4344.
40. Oliveira HS, Oliveira LCA, Pereira MC, Ardisson JD, Souza PP, Patricio PO, et al, Nanostructured vanadium-doped iron oxide: catalytic oxidation of methylene blue dye. New J. Chem. 2015; 39:3051.
41. Xiong R, Wang Y, Zhang X, Lu C, Facile synthesis of magnetic nanocomposites of cellulose@ultrasmall iron oxide nanoparticles for water treatment. RSC Adv. 2014; 4:22632.
42. Lin T-Y, Chen D-H, One-step green synthesis of arginine-capped iron oxide/reduced grapheme oxide nanocomposite and its use for acid dye removal. RSC Adv. 2014; 4:29357.
43. Xu Y, Baiu DC, Sherwood JA, McElreath MR, Qin Y, Lackey KH, et al, Linker-free conjugation and specific cell targeting of antibody functionalized iron-oxide nanoparticles. J. Mater. Chem. B 2014; 2:6198.
44. Sundar S, Piraman S, Greener saponin induced morphologically controlled various polymorphs of nanostructured iron oxide materials for biosensor applications. RSC Adv. 2015; 5:74408.
45. Anju M, Renuka NK, A novel template free synthetic strategy to grapheme-iron oxide nanotube hybrid. RSC Adv. 2015; 5:78648.

46. Saber O, Mohamed NH, Arafat SA, Conversion of iron oxide nanosheets to advanced magnetic nanocomposites for oil spill removal. RSC Adv. 2015; 5:72863.

47. Nallathamby PD, Mortensen NP, Palko HA, Malfatti M, Smith C, Sonnett J, et al, New surface radiolabeling schemes of super paramagnetic iron oxide nanoparticles (SPIONs) for biodistribution studies. Nanoscale 2015; 7:6545. https://doi.org/10.1039/c4nr06441k PMID: 25790032

48. Xu J, Wang K, Zu SZ, Han BH, Wei Z, Hierarchical Nanocomposites of Polyaniline Nanowire Arrays on Graphene Oxide Sheets with Synergistic Effect for Energy Storage. ACS Nano 2010; 4:5019. https://doi.org/10.1021/nn1006539 PMID: 20795728

49. Hussain MM, Rahman MM, Asiri AM, Ultrasensitive and selective 4-aminophenol chemical sensor development based on nickel oxide nanoparticles decorated carbon nanotube nanocomposites for green environment. J. Environ. Sci. 2017; 53:27.

50. Hussain MM, Rahman MM, Asiri AM, Non-enzymatic simultaneous detection of L-glutamic and uric acid using mesoporous Co_3O_4nanosheets. RSC Adv. 2016; 6:80511.

51. Hussain MM, Rahman MM, Asiri AM, Sensitive L-leucine sensor based on a glassy carbon electrode modified with SrO nanorods. Microchim. Acta 2016; 183:3265.

52. Rahman MM, Hussain MM, Asiri AM, A glutathione biosensor based on a glassy carbon electrode modified with CdO nanoparticle-decorated carbon nanotubes in nafion matrix. Microchim. Acta 2016; 183:3255.

53. Rahman MM, Hussain MM, Asiri AM, A novel approach towards hydrazine sensor development using SrO.CNT nanocomposites. RSC Adv. 2016; 6:65338.

54. Khayaian G, Hassanpoor S, Azar ARJ, Mohebbi S, Spectroscopic determination of trace amounts of Uranium (VI) using modified magnetic iron oxide nanoparticles in environmental and biological samples. J. Braz. Chem. Soc. 2013; 24:1808.

55. Prakash R, Fanselau K, Ren S, Mandal TK, Kubel C, Hahn H, et al, A facile synthesis of a carbon-encapsulated Fe_3O_4 nanocomposite and its performance as anode in lithium-ion batteries. Beilstein J. Nanotechnol. 2013; 4:699. https://doi.org/10.3762/bjnano.4.79 PMID: 24205466

56. Liu C, Zhang Y, Jia J, Sui Q, Ma N, Du P, Multi-susceptible single-phased ceramics with both considerable magnetic and dielectric properties by selective doping. Sci. Rep. 2015; 5:9498. https://doi.org/10.1038/srep09498 PMID: 25835175

57. Faisal M, Khan SB, Rahman MM, Jamal A, Asiri AM, Abdullah MM, Synthesis, characterizations, photocatalytic and sensing studies of ZnO nanocapsules. App. Sur. Sci. 2011; 258:672.

58. Zhang Y, Cui Z, Li L, Guo L, Yang S, Two-dimensional structure Au nanosheets are super active for the catalytic reduction of 4-nitrophenol, Phys. Chem. Chem. Phys. 2015; 17:14656. https://doi.org/10.1039/c5cp00373c PMID: 25971868

59. Liu J, Chen H, Lin Z, Lin JM, Preparation of surface imprinting polymer capped Mn-doped ZnS quantum dots and their application for chemi-luminescence detection of 4-Nitrophenol in tap water. Anal. Chem. 2010; 82:7380. https://doi.org/10.1021/ac101510b PMID: 20701302

60. Rahman MM, Khan SB, Asiri AM, Fabrication of Smart Chemical sensors Based on Transition-doped-semiconductor Nanostructure Materials with μ-Chips. PLoS ONE 2014; 9:e85036. https://doi.org/10.1371/journal.pone.0085036 PMID: 24454785

61. Rahman MM, Khan SB, Asiri AM, A microchip based fluoride sensor based on the use of CdO doped ferric oxide nanocubes. Microchim. Acta 2015; 182:487.

62. Rahman MM, Khan SB, Asiri AM, Chemical sensor development based on polycrystalline gold electrode embedded low-dimensional Ag_2O nanoparticles. Electrochim. Acta 2013; 112:422.

63. Fan Y, Liu J, Yang C, Yu M, Liu P, Graphene–polyaniline composite film modified electrode for voltammetric determination of 4-aminophenol. Sens. Actuators B 2011; 157:669.

64. Vilian ATE, Veeramani V, Chen SM, Madhu R, Huh YS, Han YK, Preparation of a reduced grapheme oxide/poly-$_L$-glutathione of 4-aminophenol in orange juice samples. Anal. Methods 2015; 7:5627.

65. Hussain MM, Rahman MM, Asiri AM, Efficient 2-nitrophenol chemical sensor development based on Ce_2O_3 nanoparticles decorated CNT nanocomposites for environmental safety. PLoS ONE 2016; 11: e0166265. https://doi.org/10.1371/journal.pone.0166265 PMID: 27973600